

Mechanism for Anaphase B: Evaluation of “Slide-and-Cluster” versus “Slide-and-Flux-or-Elongate” models.

Ingrid Brust-Mascher, Gul Civelekoglu-Scholey, Jonathan M. Scholey
Department of Molecular and Cell Biology,
University of California at Davis, Davis, CA 95616, USA.

Supporting Material

Experimental Methods.

Drosophila Stocks

Flies were maintained and embryos were collected as described previously (1, 2). Experiments were performed on embryos expressing green fluorescent protein (GFP)::tubulin (provided by Dr. Thomas Kaufman, Indiana University Bloomington), GFP::EB1 (provided by Steve Rogers, Univ. of North Carolina at Chapel Hill) or GFP::patronin (3).

Time Lapse and Fluorescent Speckle Microscopy (FSM)

Time-lapse images were acquired on an inverted microscope (IX-70; Olympus) equipped with an UltraView spinning disk confocal head (PerkinElmer-Cetus), a 100X 1.35NA objective, and an Orca ER CCD camera (Hamamatsu) using Volocity software (PerkinElmer-Cetus). A single confocal plane was acquired at time intervals of 0.5 to 2s at room temperature. For FSM, embryos were injected with rhodamine labeled tubulin (Cytoskeleton, Denver, Co). Images were analyzed with Metamorph Imaging software (Universal Imaging, West Chester, PA).

Fluorescence Recovery After Photobleaching (FRAP)

FRAP experiments were carried out on a laser-scanning Olympus confocal microscope (FV1000) with a 60×1.40 NA objective at 23°C, and images were acquired using the Fluoview software (version 1.5; Olympus). A 405 nm laser at 40% power was used to photobleach small circular regions in different areas of the spindle. Images were acquired with a 514 nm laser at rates of 4 to 5 frames per second. All data were corrected for photobleaching and normalized by $I(t) = [F(t) T_{pre}] / [T(t) F_{pre}]$, where $F(t)$ and $T(t)$ are the mean fluorescence in the FRAP region and in the entire spindle at time t , and F_{pre} and T_{pre} are the mean fluorescence in the FRAP region and in the entire spindle just before the bleach (4, 5). The recovery curve was fitted with a double exponential equation $F_{fit}(t) = F_0 + F_1(1 - e^{-k_1 t}) + F_2(1 - e^{-k_2 t})$, where $k_{1/2}$ are constants describing the rate of recovery, F_0 is the fluorescence immediately after the bleach and $F_{inf} = F_0 + F_1 + F_2$ is the maximum recovered fluorescence. The recovery half-times were calculated as $t_{1/2} = \ln 2/k$ and the percentage of fluorescence recovery was given by $(F_{inf} - F_0) / (F_{pre} - F_0)$. The fast initial recovery is due to diffusion of free tubulin and is not relevant for testing the models.

Modeling Methods.

Motor-protein generated forces on the MTs:

We assume that motor-proteins are characterized by linear force-velocity relationships (6, 7):

$f = F_m \left(1 - \frac{v}{V_m}\right)$, where v is the velocity of the plus-end-directed motor movement, F_m is the maximal motor force generated at stall ($v = 0$), and V_m is the ‘free’ ($F_m = 0$) sliding rate.

Force generated by the bipolar motor kinesin-5:

In all models, kinesin-5 motors, with pairs of motor heads at opposing ends of a rod, generate outward forces on antiparallel overlaps by stepping towards the plus ends of each MT, sliding them away from one another. A kinesin-5 motor on a pair of antiparallel MTs, sliding at rates $V_{sliding,1} = V_1$ and $V_{sliding,2} = V_2$ with their minus ends leading, to the left and right, respectively, will

exert a force of magnitude $f = F_m \left(1 - \frac{V_1 + V_2}{2V_m}\right)$ on both MTs. Similarly, a kinesin-5 motor on a

pair of MTs overlapping parallel and moving at rates V_1 and V_2 , respectively, will exert a force

$f = F_m \left(\frac{V_1 - V_2}{2V_m}\right)$ of opposite direction on the MTs, slowing down the faster MT and accelerating the slower one.

Force generated by a minus-end directed motor, Dynein or Ncd:

The minus-end directed motors in the SAC model are assumed to diffuse (or walk) along the lattice and bind to MT minus-ends at their tail-end for active force generation when their motor heads come in contact with other MTs. Thus, it is assumed that when a minus-end directed motor bound to the minus-end of a MT moving at rate V_1 , comes in contact with another parallel-aligned MT moving at rate V_2 , the minus-end motor instantly binds to and walks towards its minus end. In this way, the MT along which the motor is stepping is pulled inward (towards the spindle equator), while the MT that the minus-end directed motor is bound to at its tail-end is transported and pushed outward. The force generated by a single minus-end directed motor on

MTs sliding at rates V_1 and V_2 is $f = F_m \left(1 - \frac{V_1 - V_2}{V_m}\right)$, where $V_1 - V_2$ is the stepping rate of the

motor on its track, and force of equal magnitude is exerted on both MTs, in opposing directions.

Assuming that the motor generated forces are additive (equal load sharing) for n number of minus end directed motors per MT minus end, the total force generated at the MT’s minus end is $F = n f$.

Consequently, the minus end directed motor pulls the MTs whose minus-ends are farthest from the spindle equator inward because: (i) they mostly serve as tracks for motors bound to the minus-ends of other MTs, and (ii) the motors bound to their own minus-ends are unlikely to overlap with adjacent MTs, to walk along and to be transported and pushed outward. In contrast with that, the minus end directed motor pushes the MTs whose minus ends are near the equator outward because: (i) motors bound to their minus-ends are likely to find adjacent MT tracks to move along, to be transported and pushed outward, and (ii) there are fewer MT minus-ends near the equator, hence fewer minus-end directed motors to use them as tracks to walk along and pull them inward. This mechanism thus leads to a cooperative action of kinesin-5 and minus-end directed motors near the equator, but this cooperation is progressively lost towards regions away from the equator, and where motors balance one another, MTs' minus-ends remain immobile, forming the spindle poles.

Computational Framework and Numerical Methods:

In this section, we will describe the computational model framework, numerical methods and the algorithm used for solving the FB equations.

Computational FB Model and Numerical Solutions:

Our computational force-balance model describes a system of dynamic MTs and motors (bipolar kinesins, minus-end directed motors, and kinesin-13 depolymerases) acting on parallel and antiparallel MT overlaps and/or MT minus ends to generate forces on the MTs and the spindle poles or to depolymerize MT minus ends. In the computational model MTs are nucleated from seeds spread throughout the spindle. A pre-determined and equal number of MT nucleation seeds are allowed in each half spindle (typically 300-1000) and MTs grow towards the spindle equator from these seeds to form transient parallel and/or antiparallel overlaps. The minus end directed motors are assumed to bind instantly to newly nucleated MT minus ends at their tail end. The bipolar motors are assumed to instantly bind to dynamic MT overlaps (parallel and antiparallel) as they form. As a result of the forces generated by multiple motors MTs slide inwards or outwards. All MTs undergo MT dynamic instability (DI) at their plus ends and, when applicable, depolymerize at their pole associated minus ends as a result of the action of kinesin-13 depolymerases. In our computational model, at every time step, we keep track of each MT's plus and minus end positions and the positions of the spindle poles. All random events described below are implemented by using the built-in uniform random number generating function *rand* in MATLAB™, unless otherwise specified.

Initial conditions. In our models, at the initial time step ($t=0$) typically 600 MTs of random lengths ranging between 0.5 and 4 μm are positioned randomly, with their minus ends at most 2 - 5 μm away from the spindle equator (i.e. the spindle is initially at most 4-10 μm long). The position of the spindle poles is defined as the farthest position of the MT minus ends in each half spindle region. An initial dynamic randomly state is assigned to each MT plus end.

MT plus end dynamics. As previously described (8, 9) the dynamics of MT plus ends is computed in a Monte Carlo approach. At any given time, the MTs are either in a growth or a shrinkage state and their dynamics is fully described by the four parameters of dynamic instability: v_g , v_s , f_{cat} , and f_{res} . The growth/polymerization and shrinkage/depolymerization rates are fixed. The catastrophe and rescue frequencies are generally fixed, but one or both are re-assigned new fixed or spatially dependent values for the transition to spindle elongation. At each time step, first the new dynamic state of each MT is computed: for each MT plus end undergoing growth (or shrinkage) in the previous time step, a catastrophe (or rescue) event occurs if a random number r satisfies $r < P_{cat}(x) = 1 - \exp(-f_{cat} \Delta t)$ (or if $r < P_{res} = 1 - \exp(-f_{res} \Delta t)$) where Δt is the simulation time step. Once the state of each MT tip is determined in the current time step, the growth/shrinkage events of MT tips is executed and their new positions are computed. In addition, if a MT plus tip reaches the opposing pole it switches to shrinkage. If a MT shrinks to its seed, a new randomly chosen seed position is assigned in the same half spindle. In the “Slide and Cluster” model, the new random seed position is biased towards the spindle equator. This is implemented by a step change in the nucleation rate at a fixed distance away from the spindle equator (typically $nucl_{distance} = 2 \mu m$), and a fixed step increase in nucleation rate across this position (typically $nucl_{fold} = 3$), higher near the spindle equator. For each such event, two random numbers are selected: r_1 and r_2 . If $r_1 < 1/(nucl_{fold} + 1)$, then the seed position is outside the low nucleation region (between the spindle pole and up to $nucl_{distance}$ to the spindle equator) otherwise it is within the high nucleation region (within $nucl_{distance} \mu m$ around the spindle equator, in the appropriate spindle half). The second random number, r_2 , is used to determine the random position of the seed within the assigned low/high nucleation region of the spindle (e.g. in the left half spindle, $LowNucleationRegion = [left_{pole}, equator - nucl_{distance}]$ and $HighNucleationRegion = [equator - nucl_{distance}, equator]$).

MT minus end dynamics. As previously described (8) in the SAFE model and the Combined model, MT minus ends that come into contact with the spindle poles are depolymerized at rate v_{depoly} during preanaphase, restricting the exertion of force on the spindle poles by outward sliding MTs.

Algorithm. At each time step, first the current parallel and antiparallel MT overlaps are computed and the number of motors on each overlap is updated based on the number of motors per parallel, anti-parallel unit overlap length (k_p and k_{ap} , respectively), and the actual length of overlap, and stored. Then, the large coupled set of FB and kinematic equations for all MT mini-bundles, as described above, is set up using the current number of motors and MT overlaps, and solved. The solution to these equations yields the instantaneous velocity of all parallel and antiparallel overlapping MTs ($V_i(t)$) and the left and right spindle poles ($V_L(t)$ and $V_R(t)$) based on the force exerted on each MT and on the spindle poles. Next, assuming that non-overlapping ‘free’ MTs in the spindle move at the average rate of MTs in their vicinity, the spindle is partitioned into four equal length quarters between the poles, and an instantaneous (current time step) average velocity of MTs in each spindle quarter is computed as the mean velocity of all the parallel and

antiparallel overlapping MTs whose mid-points are within the quarter in question. Then, the instantaneous velocity of MTs that do not overlap with any other adjacent MT are assigned and stored as the average MT velocity associated with the spindle quarter their mid-point is located at. Next, the time step is incremented and the minus and plus end positions of all MTs, and the positions of the spindle poles are updated using the computed velocities. Subsequently, the dynamic states and growth/shrinkage rates of the MT plus ends are computed using the updated positions of the MTs, and based on the kinetic -rates and states of each MT plus end, and the dynamics is executed by repositioning the MT plus ends according to the event and rate of each MT plus end. If the MT minus ends are assumed to undergo depolymerization in the model considered, the new positions of MT minus ends due to depolymerization at the spindle poles are computed and updated. In the new time step, with the new positions of MTs' plus and minus ends, the new parallel and antiparallel overlaps are computed and the sequence of steps described above is repeated.

All models are solved using custom made MATLAB™ codes, run on a personal laptop computer.

Supplementary Figures

Figure S1: In the SAC model both rate and extent of elongation depend on the change in plus end dynamics. The black curve is the same as that shown in Figure 4B, obtained with the parameters shown in Tables 2 and 3. The rate of elongation is approximately the same as observed in vivo, however the extent is too long. Smaller changes in DI parameters lead to smaller spindles, but the rate of elongation is too slow.

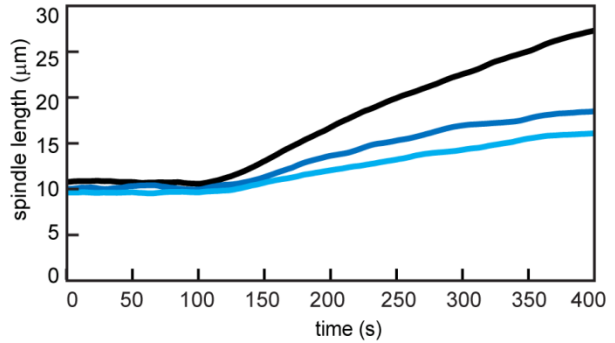
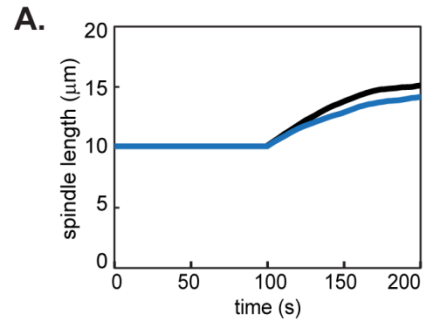


Figure S2: Spindle elongation occurs without a change in dynamics in the SAFE model, however the observed FRAP changes do not. (A) Spindle length as a function of time. The black curve is the same as that shown in Figure 5, obtained with the parameters shown in Tables 2 and 3. The blue curve is obtained without a change in dynamic instability at anaphase B onset. (B) FRAP parameters during anaphase B.



B.

	Equator		Pole	
	Half time	Percent recovery	Half time	Percent recovery
Experimental Data	5.0 ± 2.8 N=31	100 ± 11	7.0 ± 2.8 N=41	86 ± 11
Model				
SAFE with change in DI parameters	5.9 ± 1.4	102 ± 8.8	8.7 ± 1.9	84 ± 10
SAFE with no change in DI parameters	6.8 ± 1.4	98 ± 12	10.3 ± 2.4	93 ± 12

Figure S3: Effect of changes in the bipolar motor parameters on spindle length for the SAC (left) and SAFE (right) models. In all cases the blue curve is the curve obtained with the parameters in Tables 2 and 3 and shown in Figures 4B and 5. Parameters were decreased (red curve) or increased (green curve) to the values shown in the legends. In both models spindle length is sensitive to the maximal velocity.

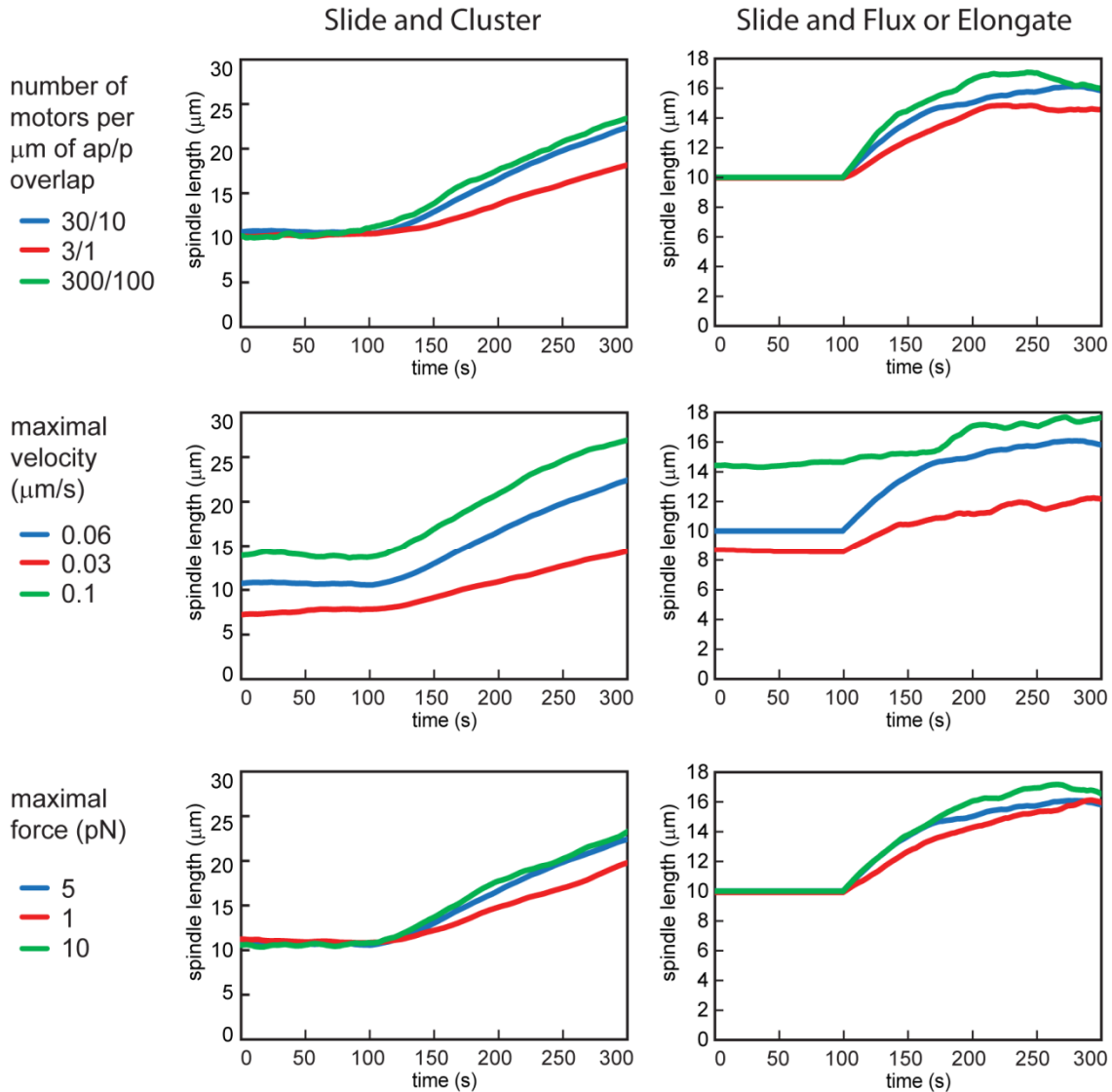
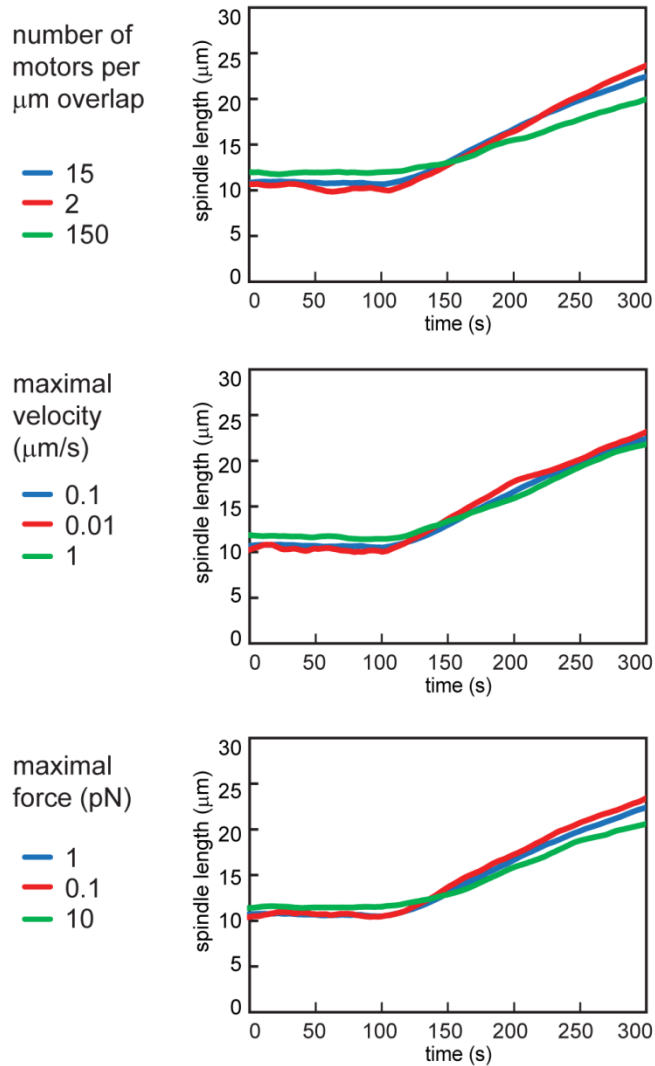


Figure S4: The spindle length in the SAC model is relatively insensitive to changes in the minus end directed motor parameters. In all cases the blue curve is the curve obtained with the parameters in Tables 2 and 3 and shown in Figure 4B. Parameters were decreased (red curve) or increased (green curve) to the values shown in the legends.



Supporting References

1. Brust-Mascher, I., G. Civelekoglu-Scholey, and J. M. Scholey. 2014. Analysis of mitotic protein dynamics and function in *Drosophila* embryos by live cell imaging and quantitative modeling. *Methods Mol Biol* 1136:3-30.
2. Sharp, D. J., K. L. McDonald, H. M. Brown, H. J. Matthies, C. Walczak, R. D. Vale, T. J. Mitchison, and J. M. Scholey. 1999. The bipolar kinesin, KLP61F, cross-links microtubules within interpolar microtubule bundles of *Drosophila* embryonic mitotic spindles. *J Cell Biol* 144:125-138.
3. Wang, H., I. Brust-Mascher, G. Civelekoglu-Scholey, and J. M. Scholey. 2013. Patronin mediates a switch from kinesin-13-dependent poleward flux to anaphase B spindle elongation. *J Cell Biol* 203:35-46.
4. Lele, T. P., and D. E. Ingber. 2006. A mathematical model to determine molecular kinetic rate constants under non-steady state conditions using fluorescence recovery after photobleaching (FRAP). *Biophys Chem* 120:32-35.
5. Phair, R. D., and T. Misteli. 2000. High mobility of proteins in the mammalian cell nucleus. *Nature* 404:604-609.
6. Valentine, M. T., P. M. Fordyce, T. C. Krzysiak, S. P. Gilbert, and S. M. Block. 2006. Individual dimers of the mitotic kinesin motor Eg5 step processively and support substantial loads in vitro. *Nat Cell Biol* 8:470-476.
7. Toba, S., T. M. Watanabe, L. Yamaguchi-Okimoto, Y. Y. Toyoshima, and H. Higuchi. 2006. Overlapping hand-over-hand mechanism of single molecular motility of cytoplasmic dynein. *Proc Natl Acad Sci U S A* 103:5741-5745.
8. Brust-Mascher, I., G. Civelekoglu-Scholey, M. Kwon, A. Mogilner, and J. M. Scholey. 2004. Model for anaphase B: role of three mitotic motors in a switch from poleward flux to spindle elongation. *Proc Natl Acad Sci U S A* 101:15938-15943.
9. Cheerambathur, D. K., G. Civelekoglu-Scholey, I. Brust-Mascher, P. Sommi, A. Mogilner, and J. M. Scholey. 2007. Quantitative analysis of an anaphase B switch: predicted role for a microtubule catastrophe gradient. *J Cell Biol* 177:995-1004.